

Nociceptor activation and damage by pulsed E-Fields.

Deepti Nene^a, Nan Jiang^b, Kristofer K. Rau^c, Martin Richardson^d and Brian Y. Cooper^e

^aDept. of Electrical and Computer Engineering, Univ. of Florida, Gainesville, FL, 32610

^{b,c}Dept. of OMFDS, Div. of Neuroscience, UCD, Univ. of Florida, Gainesville, FL, 32610

^cDept. of Neuroscience, College of Medicine, Univ. of Florida, Gainesville, FL, 32610

^dLaser Plasma Laboratory, 4000 Central Florida Dr., Orlando, FL, 32826

ABSTRACT

We assessed the capacity of ultrashort E-fields to activate rat cutaneous nociceptors. Experiments were conducted *in vitro* on nociceptive neurons representing hairy skin and glabrous skin. Electrical and optical recording methods were used to assess action potentials and membrane damage thresholds. Strength duration (SD) curves were formed for E-field pulses from 500 μ sec to 350 ns. There were no differences in the SD time constant (τ_c , 59 μ sec) or ultrashort thresholds (129 V/cm at 350 ns) for hairy or glabrous skin nociceptors, for nociceptors with distinct geometry or for nociceptors expressing different combinations of voltage sensitive Na^+ channels (TTX_s and TTX_r , Na_v) or hyperpolarization activated channels (HCN ; I_H). Subthreshold activation was possible with high frequency pulsing at ultrashort durations (350 ns; 4,000 Hz). Relative to single pulse thresholds, activation threshold could be reduced over 50% by high frequency burst trains (4,000 Hz; 1-40 msec). Nociceptors were not damaged by E-field activation. Irreversible membrane disruption occurred at significantly higher field strength and varied by cell radius (3,266-4,240 V/cm, 350 ns, 40 Hz, 5 sec). Pulse frequency had no influence on acute membrane failure (10, 20, 40, 4,000 Hz; 5 sec).

Keywords: nociceptor, ultrashort, UWB, E-field, strength-duration, cytotoxic

1. INTRODUCTION

The spatial, temporal and intensive interaction of E-fields with excitable neural membranes has been a subject of extensive modeling¹. In their simplest form, 'linear' models can be used to predict the relationship between stimulus duration and the stimulus strength required to evoke a liminal sensory or motor event (e.g., action potential, percept, movement). Strength-duration (SD) curves are formed to describe the relationship between electrical stimulation and either neural activation, or the liminal sensory percepts or motor responses that accompany them. The exponential functions fit to these observations are classically described by time constants (τ_c). The value of τ_c can vary considerably from report to report¹ (see Table 7.1), and the notion that a single value would be identified that is characteristic of neural activation has not been realized. Experimental conditions are likely to contribute to this variability². Axonal and cellular geometries will differ in distinct tissues (muscle, skin) and the complex resistive and capacitive networks of the connective tissue of skin, muscle and nerve will contribute to divergences between a nominal and effective stimulus. Moreover, the peripheral nervous systems (PNS) is composed of distinct populations of sensory afferents and motor efferents whose electrosensitive channels (e.g., Na_v) vary in distribution, voltage dependence and kinetics and may coexist with other voltage sensitive channels (I_H , I_m , K_{ir})^{3,4,5} and K^+ leak channels (TASK)⁶ that could influence field sensitivity. Protein composition may become especially significant at ultrashort field durations where peak fields are unable to couple directly to voltage sensitive residues of these proteins.

Nociceptors are a highly specialized subpopulation of the peripheral afferent pool. Nociceptors form that component of the peripheral nervous system that has evolved to transmit the neural codes that underlie noxious sensation. Our

laboratory has been devoted to the identification and characterization of specialized subpopulations of nociceptive afferents. Using a combination of cell diameter and physiological signatures associated with voltage gated channels, we have classified at least 10 nociceptive subpopulations belonging to either the IB4 positive, unmyelinated C fiber family or Nf_m positive myelinated (presumptive A δ) family of nociceptors. Specified as numeric 'types' by a set of simple classification rules (type 1, 2, 4, 5, 6, 7, 8a, 8b, 9 and 13), these nociceptive classes have been shown to be internally uniform with respect to proton receptors (ASIC), capsaicin/heat receptors (TRPV1, TRPV2), ATP receptors (P2X₁, P2X₂, P2X₃), acetylcholine receptors (α_7 , $\alpha_3\beta_4$, $\alpha_3\beta_4\alpha_5$), opiate receptors (μ , κ , δ), K⁺ leak conductances, H-currents and the expression of pro-inflammatory neuropeptides (SP and CGRP)^{7-11 12}. Recent investigations have demonstrated that specific subsets of this complex nociceptive pool innervate discrete tissues. Using fluorescent tracers injected into skin, muscle and viscera, we have observed an exceptional target specificity. A portion of the classified subpopulations innervate hairy skin exclusively (types 2, 4) while others were devoted selectively to the innervation of glabrous skin (type 13; palms of hands, soles of feet)¹². One population was shown to innervate both superficial and deep regions (type 8), either as a generic nociceptor or perhaps due an association with blood vessels. Those populations innervating superficial skin are of particular interest as they are most accessible to brief, exogenous, E-fields.

In vitro preparations create conditions in which the relationship between an E-field stimulus and the target are well defined. Fluids of known, stable conductivity couple fields to discrete cells of known geometry. The voltage dependent proteins that contribute to action potential (AP) discharge or various leak conductances can be determined and their contribution to discharge assessed. In the experiments described below, we formed SD curves for cutaneous heat sensitive nociceptors that were isolated and characterized *in vitro*. E-fields durations extended into the ultrashort (nanosecond) regime¹³, and the differential contribution of H-currents and Na_v to action potential (AP) threshold were assessed.

2. METHOD

2.1 Preparation of Cells

Young adult male Sprague-Dawley rats (90-110 g) were anesthetized with halothane and rapidly decapitated. The thoracic and lumbar dorsal root ganglia were dissected free and digested in a solution containing 5 mg/ml dispase and 2 mg/ml collagenase. Dispersed cells were plated onto 35 or 50 mm petri dishes (MatTek) as previously described⁸. Plated cells were bathed continuously in Tyrode's solution, containing (in mM) 140 NaCl, 4 KCl, 2 MgCl₂, 2 CaCl₂, 10 glucose, and 10 HEPES, adjusted to pH 7.4 with NaOH. Recordings were completed within 2-10 h after plating. Only one cell was used per petri dish. The bath was maintained at 31°C by an indium oxide coated plate (HI55D) that was feedback controlled by a TC_{bip} bath controller (Cell Microsystems). All animals were housed in American Association for Accreditation of Laboratory Animal Care-approved quarters, and all procedures were reviewed and approved by the local Institutional Animal Care and Use Committee.

2.2 Recordings

Conventional patch techniques were used to achieve the whole cell mode. Electrodes (2-10 megohm) formed from borosilicate or lime glass stock were filled with (in mM) 120 KCl, 5 Na₂-ATP, 0.4 Na₂-GTP, 5 EGTA, 2.25 CaCl₂, 5 MgCl₂, 20 HEPES, adjusted to pH 7.4 with KOH. Cells were classified according to the pattern of voltage activated currents evoked by up to three protocols^{7, 11, 14}. Voltage activated Na⁺ channels were isolated in a solution containing (in mM) 50 NaCl, 112.5 TEA, 2 CaCl₂, 0.1 CdCl₂ and 10 HEPES, adjusted to pH 7.4 with TEA-OH. For Na⁺ current isolation, the pipette solution contained 140 CsFl, 10 NaCl, 1 EGTA and 10 HEPES, adjusted to pH 7.4 with CSOH. For activation by fields of 50-500 μ sec, pulses and patterns were formed by a Grass S88. Field pulses were isolated by a transformer (SIU8T; Grass Instruments), and delivered through gold plated planar electrodes (3X5 mm Genepaddles, Harvard Apparatus) that straddled the recorded cell with a separation of 10 mm (figure 1a). At a fixed duration, thresholds were determined by two single pulse applications separated by about 1 sec. Intensity was increased in 10 V/cm steps until two action potentials were obtained at a given level. Threshold was then confirmed by stepped reduction and increase. For 350 ns fields, optical recordings were obtained with a 464 photodiode array (Neuroplex; Redshirt Imaging; 40X, .95 NA). Ca⁺⁺ fluxes were detected by Fluo-4 pentapotassium (400 μ M; 480/505/535 nm) contained within the pipette solution. Whole cell recordings preceded optical records for cell classification and Fluo-4 dialysis (4-10 megohm electrodes). After cell categorization, the amplifier was powered down and the head stage disconnected to protect the amplifier from transients. Pulse duration and frequency was controlled by a Quantum pulse former (model 9512) that triggered a high voltage pulser (Cytopulse, CT401). Current and voltage were monitored by

an Agilent, Infinium 54833A. Thresholds were determined as above with steps of 16.6 V/cm with a Genepaddle separation of 20 or 30 mm.

2.3 Electroporation

After cell categorization via electrical recordings (8-20 megohms), the amplifier was powered down and the head stage disconnected. Propidium iodide was added to the dish after the whole cell mode was achieved (100 μ M; 10 ml) and continuously thereafter (2 ml/minute). Intense E-fields were presented via gold plated electrodes positioned equidistant from the targeted cell (figure 1b). The pulse patterns (described below) were formed and monitored by the Grass S-88, Quantum, CT401 and Agilent configuration described above. Fluorescent records were captured by a Incyte software, employing a Bentham FSM150Xe monochromometer and Pixelfly CCD camera.

2.4 Immunocytochemistry

Recorded cells were processed for the presence of both TRPV1 and TRPV2 immunoreactivity. Primary antisera for TRPV1 (1:2000 guinea pig anti-vanilloid receptor 1; Novus Biologicals) and TRPV2 (1:10,000 rabbit anti-VRL-1; Chemicon International) were incubated on the cells overnight. After rinsing, secondary antisera for TRPV1 (1:100 Alexa 594 goat anti-guinea pig IgG conjugate; Molecular Probes) and TRPV2 (1:500 biotinylated goat anti-rabbit IgG; Jackson Immunoresearch Laboratories, Inc.) was applied for three hours. The biotinylated secondary antibodies were then incubated with the VectaStain Elite ABC[®] (ABC kit; Vector Laboratories) reagent kit for 30 min. Subsequently, the cells were incubated in a 1:100 dilution of a tyramide signal-amplification (TSA) kit conjugated to biotin (Perkin Elmer) for 5 min, and then a 1:100 dilution of avidin-Alexa 488 (Molecular Probes) for 40 min. Appropriate controls were performed to ensure accuracy of the method.

3. RESULTS

All experiments were conducted on subclassified nociceptor populations that have been shown to differentially innervate hairy (type 2, 4 and 8) and glabrous skin (type 8 and 13)^{10 12}. Types 2, 13 and 8 are known to be capsaicin sensitive^{7 11}. We further linked this group of nociceptors to burning sensations by identifying one or more species of heat sensitive proteins that were expressed within each subpopulation (figure 1c). Type 2 neurons expressed TRPV1 exclusively. Type 4 neurons expressed only TRPV2. The remaining two subgroups expressed both TRP proteins (figure 1c and 1d). Consistent with TRP expression, we evoked capsaizepine or ruthenium red sensitive currents in types 2, 4 and 8 by direct application of heated solutions (see figure 1e).

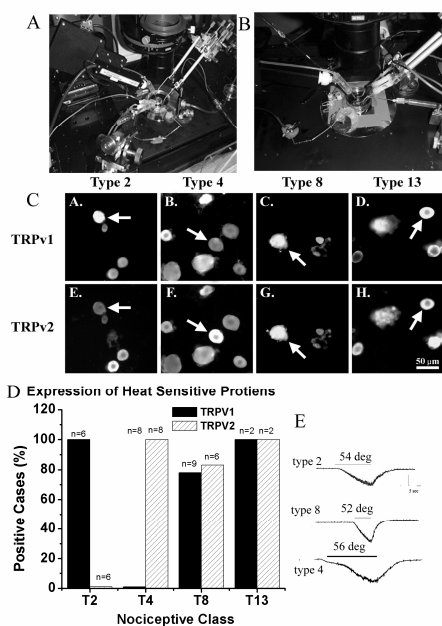


Figure 1. Field Pulsing of Heat Sensitive Cutaneous Nociceptors. **A)** For action potential recordings, nociceptive cells are plated in a petri dish. Electrical recordings are made via pipette (headstage at left) or via Ca^{++} fluorescence detected by a photodiode array (excitation through the 40X objective). The targeted cell is straddled by planar electrodes (entering at right). Threshold (at 10 Hz) is determined by the method of limits. **B)** For membrane disruption studies, nociceptive cells are isolated as described above. Electrical recordings precede the optical records (excitation through the 20X objective). Propidium iodide fluorescence (captured by CCD) is used to assess target cell membrane breakdown across a series of pulse trains of increasing field intensity. **C)** Positive immunofluorescence for TRPV1 and/or TRPV2 confirms that nociceptive classes are heat nociceptors associated with intense thermal sensation. The arrows indicate the characterized cell class identified by text above the panel. Note the other positive and negative cells in the field. **D)** Summary data indicates a consistent distribution of heat transduction proteins in the four subclasses used in field pulsing studies. **E)** Heat induced ionic current in type 2, type 4 and type 8 nociceptors. Currents are blocked by TRP antagonists ruthenium red or capsaizepine (20 and 10 μ M, respectively; not shown).

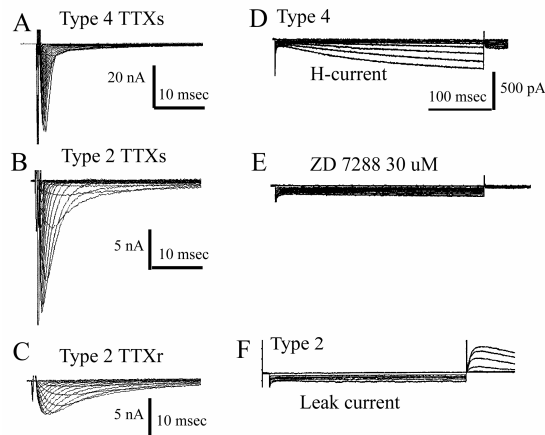


Figure 2. Distribution of Na_v and I_H in Cutaneous Nociceptors.

A) Type 4 neurons contain mainly TTXs current. A small persistent (1.9-like current) is also present (n=3; not shown). **B) and C)** Type 2 neurons express both a TTXs (B) and TTXr (C) currents (n=3). Na^+ currents were evoked by 5 mV command steps to +40 mV from a V_H of -120 mV in either the presence or absence of TTX (1 μM). Specific currents were then isolated by subtraction. **D)** Type 4 cells express large H-currents. **E)** A specific antagonist of I_H blocks the hyperpolarization activated current (ZD 7288, 30 μM ; n=5). Only leak currents remain. **F)** Only leak currents are present in type 2 cells at hyperpolarized potentials. Ba^{++} (1 mM) is present to block K_{ir} .

3.1 Diverse I_H and Na_v are Expressed in Cutaneous Heat Sensitive Nociceptors

The presence and characteristics of distinct I_H and Na_v could influence vulnerability to exogenous E-fields. The kinetics of activation, inactivation and deactivation could take on extra importance when E-fields are very brief. We used physiological and pharmacological methods to isolate and identify H-current (I_H) and Na_v in heat sensitive cutaneous nociceptors. When hyperpolarizing command steps were applied, type 4 cells exhibited a slowly activating inward current (figure 2d). Consistent with I_H , the current was completely abrogated by the specific antagonist ZD7288, (30 μM ; n= 5). It is well established that type 2 cells do not express hyperpolarization activated current^{11 15}. We were also able to identify distinct Na_v in these two classes of neurons. Using a CsFI based internal solution, Na_v could be separated into 3 distinct phenotypes based upon voltage dependence, kinetics and sensitivity to TTX. Both type 2 and type 4 cells expressed a TTX sensitive (TTXs) current with fast inactivation similar to $\text{Na}_v1.7$ ¹⁶(type 2: tau = 1.62 +/- .27 msec, n=5; type 4: tau = 0.457 +/- .03 msec, n=13, V_c =-30 mV; figure 2). Type 2 cells expressed at least two slowly inactivating TTX resistant (TTXr) currents. One of these exhibited ultraslow inactivation kinetics and a hyperpolarization shifted activation consistent with $\text{Na}_v1.9$ (tau = 20.2 +/- 3.5 msec, V_c =-50 mV, n=4). A similar persistent current was observed in type 4 cells (tau = 21.5 +/- 1.3 msec, V_c =-50 mV, n=15). In type 2, an additional TTXr current exhibited inactivation kinetics and voltage dependence consistent with $\text{Na}_v1.8$ ¹⁷ (tau = 4.65 +/- .37 msec, V_c =-30 mV, n=7; figure 2c).

3.2 Field Pulsing with Electrical Recording

We examined the relationship between short duration E-fields and action potential discharge. Experiments were conducted on 3 classes of heat and/or capsaicin sensitive cutaneous nociceptors that included identified C (type 2) and A-fiber (type 4) nociceptors¹¹. Following cell classification procedures, E-fields were presented at various durations and intensities (50-500 μsec pulse duration; I=0 mode). As expected, action potentials could be reliably evoked in both C and presumptive A δ nociceptors. Thresholds for action potentials varied by pulse duration (figure 3). AP thresholds for A δ and C nociceptors exhibited similar thresholds for pulses ranging from 50 to 500 μsec . Neither rheobase (33.1 and 31.1 V/cm) nor tau_c (41.4 and 46.6 μsec) differed for these nociceptive populations. At suprathreshold intensities, long trains of action potentials were reliably entrained (1 pulse: 1 action potential) to E-field pulses (5 to 40 Hz) for up to 10 seconds (figure 3). With intensities at threshold, increases in pulse frequency resulted in progressively lower percentage of AP entrainment. Following rates fell as low as 30 % at 40 Hz. Action potential failure rates were substantially reduced by suprathreshold stimulation. Using E-fields at twice the observed threshold, action potential entrainment approached 100% regardless of pulse frequency and train duration (n= 7 and 3; figure 3c). Resting membrane potential remained relatively stable during field stimulation protocols (50.6 +/- 0.6 vs 52.0 +/- 0.8).

3.2 Field Pulsing with Optical Recording

Optical records (Ca^{++} fluorescence) were made to expand the SD curve into the ultrashort regime. These recordings were subsequently combined with electrical recordings (types 2, 4 and 8 only) to form SD curves that spanned the range from μsec to ns.

In a series of preliminary experiments, simultaneous optical and electrical recordings were conducted to confirm the relationship between Ca^{++} fluorescence and action potential evocation. Following initial characterization procedures, the neuron was brought into current clamp mode. Subsequently, action potentials were evoked by brief current injection from the recording electrode (1 msec, 1-4 nA; 10 Hz; figure 4). One of 5 injections was chosen to be subthreshold for action potential discharge (1 nA). Simultaneous recordings of action potentials and Ca^{++} fluxes showed complete temporal and intensive overlap of suprathreshold induced action potentials and Ca^{++} flux records (n=6; figure 4). Current injections that were subthreshold for action potentials did not produce an optical Ca^{++} flux.

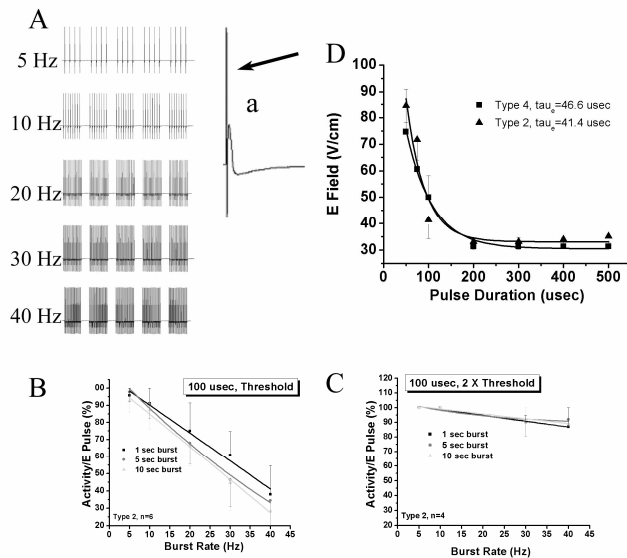
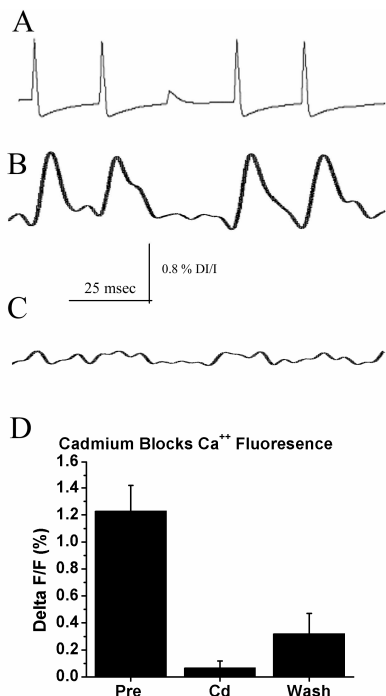


Figure 3. Field Pulsing with Electrical Recording. **A)** left: Action potentials follow high rates of pulsing that span their physiological range (5-40 Hz). In this highly condensed figure, the action potentials are the thickened portion of the traces at the baseline. **Aa)** An action potential (type 2) evoked by a field pulse (expanded from the left panel). Note the large field ‘artifact’ (arrow). **B)** At threshold intensity, nociceptors fail to follow field pulses reliably. **C)** At 2X threshold, following exceeds 90% at all frequencies. **D)** Strength-duration curves for A δ (type 4) and C (type 2) nociceptors do not differ.



As Ca^{++} fluxes can arise from external or internal sources, we used pharmacological means to identify the source of these currents. Ca^{++} fluxes from external sources are gated by voltage dependent Ca^{++} channels that can be blocked by Cd^{++} . Again, using simultaneous electrical and optical recording, we depolarized nociceptors by internal injection to produce a brief series of action potentials. Subsequently, the neuron was exposed to a Tyrode’s solution containing Cd^{++} (200 μM ; n=6). Consistent with the action potential dependent influx of extracellular Ca^{++} into the intracellular space, Cd^{++} completely abrogated optically recorded Ca^{++} signals (figure 4).

Figure 4. Action Potentials and Ca^{++} Fluxes During Combined Electrical and Optical Recordings. **A)** Action potentials evoked in a type 2 nociceptor by current injection (40 Hz). One injection is purposely subthreshold. **B)** Simultaneous optical records confirm that Ca^{++} fluorescence follows action potential discharge and corresponds mainly to the K_{ca} phase. **C)** The Ca^{++} response is completely abrogated by Cd^{++} (200 μM). **D)** Summary graph for Cd^{++} blockade (n=6). The response only partially recovers.

Using voltage dependent Ca^{++} flux as an index, we examined whether ultrashort, UWB E-fields could evoke action potentials in cutaneous nociceptors, and whether a specific form of Na_v was required for this activation. With brief, 10 Hz bursts of 350 ns (2 pulses), action potential dependent Ca^{++} flux was observed reliably in all 4 nociceptor

populations (figure 5). AP thresholds did not vary significantly between cutaneous nociceptor classes (129.4 +/- 7 V/cm; n=53), nor did they differ for A δ and C nociceptors (type 4 vs 2 and 8). Despite distinctions in Na_v content, cell geometry in types 2 (radius = 17.8 +/- .4) type 4 (radius = 23.1 +/- .3) and type 8 (radius = 24.9 +/- .9), or presence of I_H (type 4 vs type 2) there were no statistical differences in 350 ns thresholds (figure 5). Therefore, these data were combined to form a single SD curve to represent the nociceptor family. This curve yielded a tau_e of 59.2 μ sec with a rheobase of 36.2 V/cm. If the distinct threshold and kinetics of Na_v (figure 2) made nociceptors differentially vulnerable to ultrashort pulse activation, it was not apparent in these tests. The absence of threshold differences could be interpreted as a dominant role of TTXs Na_v. As we had shown that these proteins were present in both type 2 and type 4, they might mediate ultrashort activation events. To test this hypothesis we applied, by close superfusion, the Na_v specific toxin, TTX (1 μ M), to block TTXs Na_v in both populations. Following threshold determination, E-fields were presented repeatedly (threshold +25 V/cm) over a period of 5 minutes (1 min test intervals). TTX was superfused over the cell during the last 4 tests. TTX prevented AP activation in type 4 nociceptors (8/9 cases); however, activation of type 2 cells was not affected (6/6 cases; p<.004; figure 6). AP block was usually seen within 1 minute of TTX application. Repeated testing, in the absence of TTX, indicated a general decline of peak Ca⁺⁺ fluorescence over the 5 minute test period (30.0 +/- 7.0%; n=4).

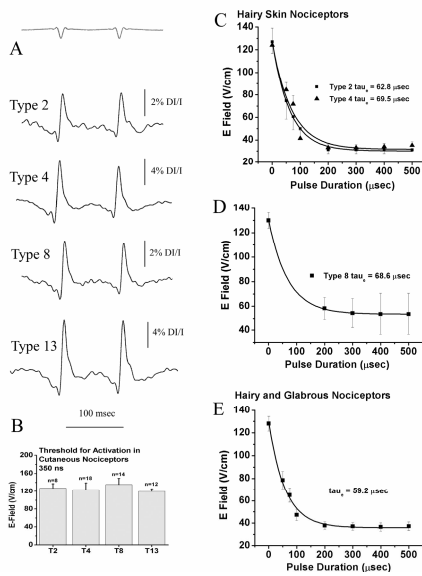


Figure 5 (left). Ultrashort Field Pulsing with Optical Recording. A) Ultrashort pulses activate cutaneous nociceptors (350 ns; 10 Hz). The stimulus monitor at the top of the panel represents the timing but not actual duration of the E-field. **B)** Threshold for activation did not differ by nociceptive subclass. **C)** Optical records merged with electrical recordings to form full SD curves for hairy skin nociceptors. **D)** Optical recordings merged with electrical recordings for glabrous skin nociceptors. **E)** SD curve for the cutaneous nociceptive pool (tau_e=59.2 usec).

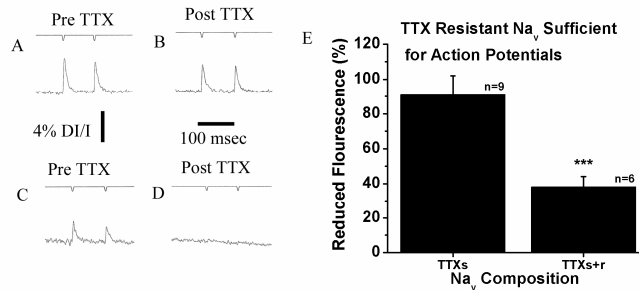


Figure 6. Both TTXs and TTXr are Ultrashort-AP Competent. Type 2 and type 4 express TTXs+r and TTXs respectively. **A) and B)** Action potentials are evoked in a type 2 nociceptor in the presence of TTX (1 μ M). **C) and D)** Action potentials are prevented by TTX in a type 4 nociceptor. **E)** Summary graph of reduced fluorescence in the presence of TTX in type 2 (TTXs+r) and type 4 (TTXs) nociceptors. A non-specific decline in fluorescence over the 5 minute test interval (see text) is consistent with decreased fluorescence in type 2 (350 ns pulses, 10 Hz).

High frequency pulsing can reduce sensory threshold^{18 19}. Models of AP evocation, based upon active membrane processes, predict that charge integration on the internal membrane will reduce AP threshold^{20 21}. Ultrashort duration, subthreshold pulses, should summate charge on the internal lipid leaflet, as long as the frequency is sufficient to overcome the discharge rate. Summation of charges will eventually reach critical levels for action potential evocation²². We examined whether nociceptor E-field activation threshold could be reduced by high frequency E-field pulsing at 350 ns. Studies were made on 4 distinct cutaneous nociceptor populations. Single pulse thresholds were first determined for a given case. Subsequently 4,000 Hz bursts were presented (1, 5, 25 or 40 msec burst duration) and thresholds were identified. When possible, we reestablished the original single pulse threshold after the high frequency tests in order to ensure that it had not changed. As predicted, the threshold for AP activation was reduced in a burst duration dependent manner. As there were no differences in nociceptor AP vulnerability, data from all 4 nociceptor populations were pooled. At 4,000 Hz, threshold was reduced up to 60% of single pulse thresholds (58.9 +/- 6 V/cm; n=13; figure 7). Potentiation of evoked discharge appeared to reach a maximal value at 5-10 msec burst durations.

Although the decrease in threshold was maximal for 40 msec bursts, these were not significantly greater than those produced by bursts of 5 or 20 msec (53%, n=9 and 54%, n=21). Despite the fact that these nociceptors expressed distinct Na_v proteins, we did not observe any differences in the vulnerability of nociceptors to high frequency, nanosecond, pulsing. In type 2 nociceptors, threshold reduction by 4,000 Hz bursts was unaffected by the presence of TTX (type 2; 5 msec burst; 1 μM ; n=2). Therefore, it appeared that TTXr Na_v were also vulnerable to subthreshold burst activation.

It was possible that the high frequency pulsing paradigm might evoke Ca^{++} release from internal Ca^{++} stores rather than external sources associated with action potential discharge^{23,24}. To examine this possibility, we used Cd^{++} (200 μM) to block external Ca^{++} fluxes through voltage dependent Ca^{++} channels. Consistent with an external Ca^{++} source, we were able to block Ca^{++} fluxes during high frequency pulsing experiments (4,000 Hz; 20 msec burst duration; 350 ns; n=7; figure 7).

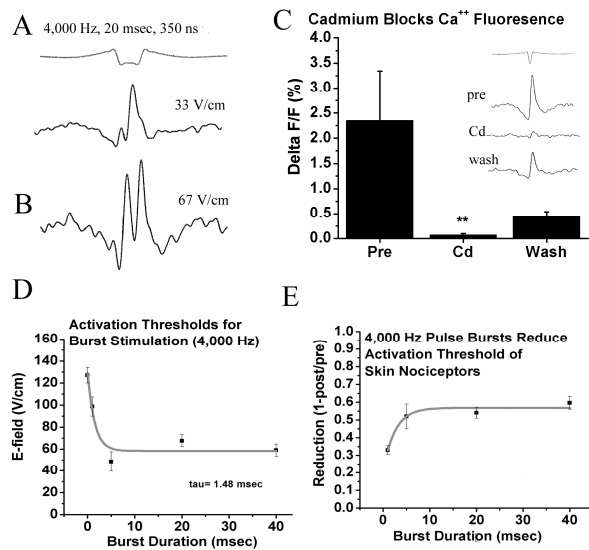


Figure 7. High Frequency Pulsing with Ultrashort E-fields Reduces Nociceptor Activation Threshold. **A)** A 4,000 Hz burst (350 ns; 20 msec) elicits an action potential Ca^{++} flux at subthreshold (single pulse) intensity. **B)** Multiple discharges are evoked at subthreshold intensity by 4,000 Hz burst. **C)** Cd^{++} blocks burst initiated discharge (n= 7). **D)** Single pulse thresholds are substantially reduced by high frequency bursts. The optimal duration of an ultrashort burst is between 5 and 10 msec. **E)** The same data as ‘D’ plotted as percentage reduction of the single pulse threshold.

3.3 Membrane Disruption

At sufficient intensity, E-fields can irreversibly disrupt cellular membranes through the exertion electromechanical forces on the polar heads of membrane lipids²⁵. These membrane damaging events are likely to occur at higher intensities than those that induce a physiological activation. We examined the capacity of 5 sec trains of intense E-fields (20, 2 and 0.350 μsec pulse duration) to irreversibly disrupt nociceptive membranes. Electrical recordings were used to classify nociceptive neurons. Subsequently, optical recordings of propidium iodide fluorescence (100 μM) were used as an indicator of membrane disruption. Intracellular fluorescence was assessed for 2 minutes following each 5 sec E-field test event (see figure 8). Irreversible disruption was defined as increasing PI fluorescence (>5%) that persisted during the final 30 seconds of the 2 minute observation period.

Relative to activation thresholds, nociceptors proved to be highly resistant to membrane disruption. Disruption was clearly distinguishable from poration by the dramatic increase in intracellular fluorescence that appeared coincident with the 5 sec train of pulses (figure 8b insert). Reversible poration was also observed as a stepped increase in fluorescence that stabilized within the 2 minute observation period (figure 8b insert). Field intensity for cytotoxic disruption was typically in the range of 3,000-4,000 V/cm. For acute cytotoxic effects, this exceeded activation thresholds by a safety factor of 20-30. However, as cells can transition to apoptosis, we cannot rule out a delayed cell death at lower E-fields, given the conditions of our experiments²⁶. Also in contrast to activation thresholds, nociceptor trauma thresholds varied by cellular geometry. At durations of 350 ns, small diameter types 2 and 13 ($r = 17.9 \pm .33$ and $17.9 \pm .36 \mu\text{M}$) were irreversibly disrupted at intensities near 4,000V/cm (figure 8). Larger diameter neurons ($r =$

21.1±.7 and 24.3±.52) exhibited disruption thresholds near 3,000 V/cm. These differences were statistically significant ($p < .05$).

High frequency pulsing can decrease poration thresholds in non-neural cells, and could provide pathways for Ca^{++} flux and AP generation^{27,28}. Accordingly, we examined whether high frequency pulsing, associated with activation threshold reduction, decreased membrane poration or disruption thresholds. Using 5 sec burst trains at 4,000 Hz (40 msec burst duration, 350 ns pulse duration), we were unable to identify any poration below 1,000 V/cm in 4 nociceptive cell classes (n=20). Nor did we observe any significant shift in threshold for irreversible membrane disruption in type 2, 4, 8 or 13 relative to those observed at 40 Hz, 5 sec (figure 8). We were also unable to increase nociceptor safety factor by low frequency pulsing (type 2, 2 usec; 10-20 Hz; figure 8).

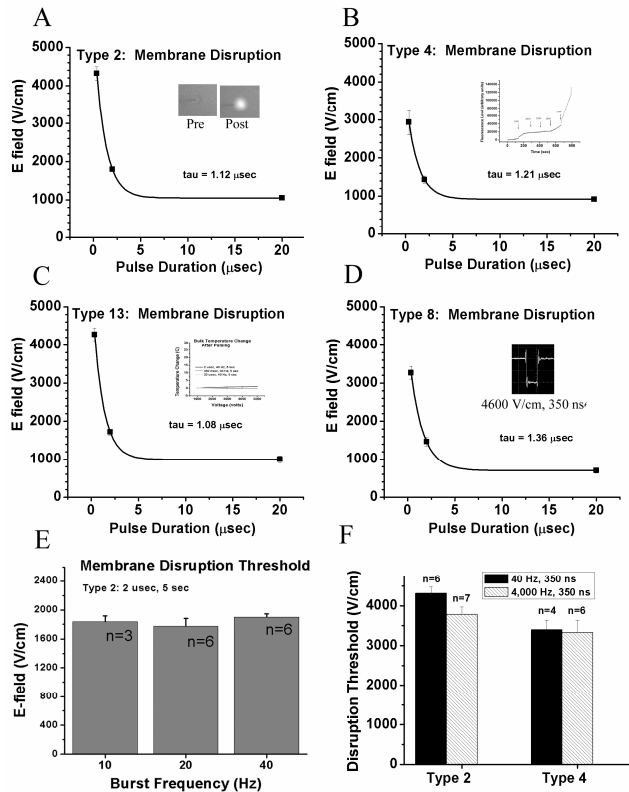


Figure 8. Irreversible Membrane Disruption in Cutaneous Nociceptors. A-D) E-fields (20-350 μsec) break down nociceptor membranes at high intensity in a duration dependent manner (40 Hz, 5 sec). In (A), the insert shows a target cell before and after pulsing at 4,000 V/cm (350 ns, 40 Hz, 5 sec). In (B), the insert shows time and intensity dependent changes in PI fluorescence in a type 4 nociceptor. Note the large and irreversible increase in PI fluorescence at 2,800 V/cm. In (C) the insert shows negligible change in bulk temperature with pulsing (40 Hz, 2 μsec , 5 sec). In (D) the insert shows a 350 ns pulse. E) Decreasing the stimulus frequency from 40 to 10 Hz does not alter the threshold for disruption at 2 μsec . F) High frequency bursts (4,000 Hz) do not alter the threshold for membrane disruption in type 2 or type 4 cutaneous nociceptors (350 ns).

4. Discussion

We examined the vulnerability and molecular basis of nociceptor activation by ultrashort, UWB E-fields. Nociceptors could be activated by pulses as short as 350 ns. The activation threshold was similar in, heat encoding, cutaneous nociceptors despite distinct cellular geometry and differential distribution of voltage sensitive H-currents and Na_v . Either TTXs Na_v or TTXr $Nav1.8$ -like currents were sufficient for ultrashort activation, and the presence or absence of H-currents had no discernable influence on AP threshold. Strength-duration curves indicated a universal τ_c of 59 μsec for superficial $A\delta$ or C nociceptors. Exogenous E-fields became cytotoxic as field intensities exceeded activation thresholds by 20-30 fold. Thresholds for neural activation could be reduced >50% with high frequency pulse protocols (4,000 Hz) with no apparent influence on membrane breakdown.

Voltage gated Na^+ channel proteins (Na_v) are responsible for initiating action potential discharge. Nociceptors contain multiple forms of Na_v (including $Na_v 1.7, 1.8$ and 1.9)^{16,29,30} whose distinct voltage sensitivity and kinetics could make them more or less vulnerable to depolarizing, ultrashort, E-fields³¹⁻³⁵. The substantial variation in Na_v kinetics could be

important for ultrashort activation. Such fields are too brief to permit direct coupling of the induced field peak to membrane proteins^{36 37}. Accordingly, AP competent peak voltage shifts are predicted to be substantially higher than nominal threshold. The exceptionally fast onset kinetics, characteristic of TTXs Na_v , could provide the rapid surge of Na^+ ions needed to create the regenerative cascade of channel openings required for action potential formation. Opposing this advantage, the rapid inactivation of TTXs Na_v could prevent materialization of sufficient fluxes over the critical time necessary for membrane proteins to respond *en masse*. Alternately, because TTXr 1.8 activates more slowly, the degree of ion flux for this channel would be limited for brief subthreshold fields. Yet the slow inactivation kinetics of TTXr 1.8 could be preferable, because ion fluxes might persist over the time frame required to initiate a self-perpetuating response. Our nociceptive populations expressed fast kinetic TTXs, and distinct combinations of TTXr. The latter included a weak, persistent Na_v 1.9-like current with a hyperpolarization shifted activation profile that may function as a Na^+ leak conductance that would not directly support action potential discharge. Also present was an Na_v 1.8-like current with slow inactivation kinetics. We tested the hypothesis that these Na_v would be differentially sensitive to ultrashort E-fields. Similar coupling thresholds were observed in all nociceptive classes (including those that were not specifically characterized for Na_v phenotype; type 8 and 13). Nociceptors expressing either AP competent TTXs (TTXs; type 4) or those expressing TTXs and AP competent TTXr 1.8 (type 2) were similarly susceptible to ultrashort E-fields. When TTX was used to block the TTXs component, action potentials were abrogated in type 4, but were unaffected in type 2 nociceptors. Therefore, either Na_v was sufficient to mediate action potentials at 350 ns.

Other voltage dependent conductances are present in nociceptors and could contribute to action potential induction by exogenous E-fields. HCN proteins combine to form hyperpolarization activated channels and possibly Na^+ leak conductances (H-current, I_H)³. Although the distribution of HCN1-4 proteins in nociceptors are not known precisely, diverse forms of these relatively slowly activating, and ultraslow deactivating, mixed Na^+ and K^+ currents, are commonly expressed in nociceptive neurons (types 4, 8 and 13)^{7 11 15}. Following hyperpolarization, H-current dependent fluxes can couple to Na_v and produce action potential discharge³. In our experiments, circular cells were exposed to E-fields via a pair of equidistant planar electrodes. In these conditions a depolarizing displacement current occurs at the cathode facing membrane, and a hyperpolarization occurs at the anode facing membrane^{38 39 40}. Our methods did not permit us to distinguish whether action potentials were initiated at the cathodal or anodal facing membrane. If hyperpolarizing currents mediated action potential discharge via H-current, then it would be expected that the absence of such current would have a substantial influence on discharge threshold. As we, and others, have previously demonstrated, type 2 nociceptors express no I_H while type 4 nociceptors express powerful H-currents. We could not detect any influence of H-current on the vulnerability of nociceptors to ultrashort E-fields. Other investigators have emphasized K_{ir} as a mediator of hyperpolarization-induced discharge at fields that exceed threshold by about 10 fold⁴⁰. We have not assessed the distribution of K_{ir} in nociceptive neurons, nor have we explored how mediating events may transition to other modes at very high field strengths.

Our cutaneous nociceptors contained representatives of the $\text{A}\delta$ (type 4) and C fiber nociceptive families (type 2 and 8). We have not fully determined the assignment for type 13 nociceptors. While we did not find any differences in E-field vulnerability for $\text{A}\delta$ and C fiber families, it cannot be concluded that distinct vulnerability, in degree, will not be found *in vivo*. Using contact electrodes and verbal report of human volunteers, $\text{A}\delta$ mediated 'fast' nociception is evoked at significantly lower thresholds than C fiber mediated 'slow' nociception⁴¹. Noxious perception is assembled across multiple levels of the nervous system, but a portion of these perceptual differences should be attributable to peripheral afferent susceptibility. Included among the numerous distinctions between the $\text{A}\delta$ and C families are conduction velocity, fiber diameter, distribution of Na_v , IB4 binding, distribution of neurofilaments, and myelinating Schwann cell association⁴². Some of these known distinctions, and others unknown, might contribute to E-field vulnerability of nociceptor families at their peripheral tissue terminations (i.e., myelination, tissue branching patterns, fiber diameter, Na_v). Because $\text{A}\delta$ fibers lose myelination as they enter their terminal sites in skin, it is unlikely that the nodal architecture of a myelinated nerve would influence exogenous E-field activation threshold. From the perspective of membrane charging, models emphasize axonal orientation and distal terminals as sites of special E-field susceptibility^{43 44 45}. Fibers that innervate human skin are extensively branched and form complex arborizations. Most of these epidermal fibers are likely to be nociceptive, but their specific membership in $\text{A}\delta$ or C fiber families are not known^{46 47 48 49}. Amid these epidermal arborizations, the specific location of action potential initiation sites are also uncertain, but evidence suggests they are likely to occur near distal terminals and reoccur at proximal branch points where membrane charging could be favorable⁵⁰. It is possible that the concentration of specific Na_v at initiation sites influences vulnerability, but there is little information regarding those specific Na_v that occupy peripheral endings and branch sites

for any nociceptive class. In our experiments, we used nociceptor cell bodies to probe for the molecular basis of E-field discharge. Cell bodies will express Na_v and other voltage sensitive channels that eventually reside in axons, cell bodies and terminals. Our observation that specific Na_v had little influence on ultrashort thresholds, indicates that these considerations may not be of great importance at 350 ns. Regardless of whether TTXs or TTXr, are expressed singly or in combination at peripheral endings or branch points would seem to be of little import, as both are similarly vulnerable to 350 ns UWB fields. Because Na_v protein expression had marginal impact, the influence of fiber thickness and terminal arborization patterns may be relatively more determinant *in vivo*. Membrane charging should substantially favor longitudinal axonal orientation paths as sites of initiation⁵¹. These may occur at branch points or as a dominant terminal site architecture. In transparent corneal membranes, termination patterns are distinct for the major nociceptive families. Highly systematic horizontal and vertical patterns can be visualized and were differentially represented by A δ and C fibers, respectively⁵². Methods to identify such architectural distinctions in skin have been stymied by significant methodological difficulties in this opaque, relatively complex tissue matrix. Because our studies were conducted *in vitro*, conditions were ideal to assess contributions of Na_v and other voltage sensitive proteins to threshold and τ_{c} . The universal susceptibility of TTXs and TTXr Na_v allays concerns about a differential distribution of voltage sensitive proteins into axonal, terminal and cell body compartments. The influence of tissue termination architecture cannot be assessed *in vitro*. Although both horizontal and vertical branches are likely to be present in all nociceptor arborizations, tissue termination patterns may be significant, and it is premature to conclude from our evidence that A δ and C fibers will not prove to be differentially vulnerable, in degree, to ultrashort E-fields. Furthermore, as the UWB component of E-fields is reduced to the picosecond regime, Na_v protein kinetics could emerge as a critical factor.

Acknowledgment

We would like to thank Rucha Nene for her valuable assistance in many phases of this project. Supported in part by NIH/NINCDS 39874 to BYC

References

1. Reilly, J.P., *Applied Bioelectricity*. 1998, New York: Springer Verlag.
2. Bostock, H., *The strength-duration relationship for excitation of myelinated nerve: computed dependence on membrane parameters*. J Physiol, 1983. **341**: p. 59-74.
3. Pape, H.C., *Queer current and pacemaker: the hyperpolarization-activated cation current in neurons*. Annu Rev Physiol, 1996. **58**: p. 299-327.
4. Brown, D.A., et al., *Muscarinic mechanisms in nerve cells*. Life Sci, 1997. **60**(13-14): p. 1137-44.
5. Isomoto, S., C. Kondo, and Y. Kurachi, *Inwardly rectifying potassium channels: their molecular heterogeneity and function*. Jpn J Physiol, 1997. **47**(1): p. 11-39.
6. Patel, A.J. and E. Honore, *Anesthetic-sensitive 2P domain K⁺ channels*. Anesthesiology, 2001. **95**(4): p. 1013-21.
7. Petruska, J.C., et al., *Chemical responsiveness and histochemical phenotype of electrophysiologically classified cells of the adult rat dorsal root ganglion*. Neuroscience, 2002. **115**(1): p. 15-30.
8. Cooper, B.Y., R.D. Johnson, and K.K. Rau, *Characterization and function of TWIK-related acid sensing K⁺ channels in a rat nociceptive cell*. Neuroscience, 2004. **129**(1): p. 209-24.
9. Rau, K.K., et al., *Diverse immunocytochemical expression of opioid receptors in electrophysiologically defined cells of rat dorsal root ganglia*. J Chem Neuroanat, 2005. **29**(4): p. 255-64.
10. Rau, K.K., R.D. Johnson, and B.Y. Cooper, *Nicotinic AChR in Subclassified Capsaicin-Sensitive and -Insensitive Nociceptors of the Rat DRG*. J Neurophysiol, 2005. **93**(3): p. 1358-71.
11. Petruska, J.C., et al., *Subclassified acutely dissociated cells of rat DRG: histochemistry and patterns of capsaicin-, proton-, and ATP-activated currents*. J Neurophysiol, 2000. **84**(5): p. 2365-79.
12. Jiang, N., et al., *The proton sensitivity, Ca²⁺ permeability and molecular basis of ASIC channels expressed in glabrous and hairy skin afferents*. J Neurophysiol, 2006.

13. Rogers, W.R.M., J.H.; Comeaux, J.A., Jr.; Kuhnel, C.T.; Moreland, D.F.; Teltschik, D.G.; Lucas, J.H.; Murphy, M.R., *Strength-duration curve for an electrically excitable tissue extended down to near 1 nanosecond*. IEEE Trans Plasma Sci, 2004. **32**(4): p. 1587- 1599.
14. Petruska, J.C., et al., *Distribution of P2X1, P2X2, and P2X3 receptor subunits in rat primary afferents: relation to population markers and specific cell types*. J Chem Neuroanat, 2000. **20**(2): p. 141-62.
15. Cardenas, C.G., L.P. Del Mar, and R.S. Scroggs, *Variation in serotonergic inhibition of calcium channel currents in four types of rat sensory neurons differentiated by membrane properties*. Journal of Neurophysiology, 1995. **74**(5): p. 1870-1879.
16. Djouhri, L., et al., *Sensory and electrophysiological properties of guinea-pig sensory neurones expressing Nav 1.7 (PNI) Na⁺ channel alpha subunit protein*. J Physiol, 2003. **546**(Pt 2): p. 565-76.
17. Lai, J., et al., *Voltage-gated sodium channels and hyperalgesia*. Annu Rev Pharmacol Toxicol, 2004. **44**: p. 371-97.
18. Notermans, S.L., *Measurement of the pain threshold determined by electrical stimulation and its clinical application. I. Method and factors possibly influencing the pain threshold*. Neurology, 1966. **16**(11): p. 1071-86.
19. Gibson, R.R., *Electrical Stimulation of Pain and Touch*. The Skin Senses, ed. D.R. Kenshalo. 1968, Springfield IL: Charles C. Thomas. 223-261.
20. Reilly, J.P., *Electrical models for neural excitation studies*. Johns Hopkins APL Tech. Digest, 1988. **9**(1): p. 44-58.
21. Bostock, H. and J.C. Rothwell, *Latent addition in motor and sensory fibres of human peripheral nerve*. J Physiol, 1997. **498** (Pt 1): p. 277-94.
22. Tasaki, I.S., M., *On the relation of the strength-frequency curve in excitation by alternating current to the strength-duration and latent addition curves of the nerve fiber*. J. Gen. Physiol., 1951. **34**: p. 373-388.
23. Vernier, P.T., et al., *Nanoelectropulse-induced phosphatidylserine translocation*. Biophys J, 2004. **86**(6): p. 4040-8.
24. Schoenbach, K.H., S.J. Beebe, and E.S. Buescher, *Intracellular effect of ultrashort electrical pulses*. Bioelectromagnetics, 2001. **22**(6): p. 440-8.
25. Joshi, R.P. and K.H. Schoenbach, *Electroporation dynamics in biological cells subjected to ultrafast electrical pulses: a numerical simulation study*. Phys Rev E Stat Phys Plasmas Fluids Relat Interdiscip Topics, 2000. **62**(1 Pt B): p. 1025-33.
26. Deng, J., et al., *The effects of intense submicrosecond electrical pulses on cells*. Biophys J, 2003. **84**(4): p. 2709-14.
27. Hair, P.S., K.H. Schoenbach, and E.S. Buescher, *Sub-microsecond, intense pulsed electric field applications to cells show specificity of effects*. Bioelectrochemistry, 2003. **61**(1-2): p. 65-72.
28. Buescher, E.S., Smith, R.R., Schoenbach, K.H., *Submicrosecond intense pulsed electric field effects on intracellular free calcium: mechanisms and effects*. IEEE Transactions on Plasma Science, 2004. **32**(4): p. 1563- 1572.
29. Fang, X., et al., *The presence and role of the tetrodotoxin-resistant sodium channel Na(v)1.9 (NaN) in nociceptive primary afferent neurons*. J Neurosci, 2002. **22**(17): p. 7425-33.
30. Djouhri, L., et al., *The TTX-resistant sodium channel Nav1.8 (SNS/PN3): expression and correlation with membrane properties in rat nociceptive primary afferent neurons*. J Physiol, 2003. **550**(Pt 3): p. 739-52.
31. Elliott, A.A. and J.R. Elliott, *Characterization of TTX-sensitive and TTX-resistant sodium currents in small cells from adult rat dorsal root ganglia*. J Physiol, 1993. **463**: p. 39-56.
32. Akopian, A.N., L. Sivilotti, and J.N. Wood, *A tetrodotoxin-resistant voltage-gated sodium channel expressed by sensory neurons*. Nature, 1996. **379**(6562): p. 257-262.
33. Tate, S., et al., *Two sodium channels contribute to the TTX-R sodium current in primary sensory neurons*. Nature (Neuroscience), 1998. **1**(8): p. 653-655.
34. Cummins, T.R., et al., *A novel persistent tetrodotoxin-resistant sodium current in SNS-null and wild-type small primary sensory neurons*. J Neurosci, 1999. **19**(24): p. RC43.
35. Dib-Hajj, S., et al., *NaN/Nav1.9: a sodium channel with unique properties*. Trends Neurosci, 2002. **25**(5): p. 253-9.
36. Dean, D. and P.D. Lawrence, *Optimization of Neural Stimuli Based Upon a Variable Threshold Potential*. IEEE Trans Biomed Eng, 1983. **32**(1): p. 8-14.

37. Barr, R.C. and R. Plonsey, *Threshold variability in fibers with field stimulation of excitable membranes*. IEEE Trans Biomed Eng, 1995. **42**(12): p. 1185-91.
38. Gross, D., L.M. Loew, and W.W. Webb, *Optical imaging of cell membrane potential changes induced by applied electric fields*. Biophys J, 1986. **50**(2): p. 339-48.
39. Hibino, M., H. Itoh, and K. Kinoshita, Jr., *Time courses of cell electroporation as revealed by submicrosecond imaging of transmembrane potential*. Biophys J, 1993. **64**(6): p. 1789-800.
40. Sharma, V., R.C. Susil, and L. Tung, *Paradoxical loss of excitation with high intensity pulses during electric field stimulation of single cardiac cells*. Biophys J, 2005. **88**(4): p. 3038-49.
41. Cooper, B.Y., C.J. Vierck, Jr., and D.C. Yeomans, *Selective reduction of second pain sensations by systemic morphine in humans*. Pain, 1986. **24**(1): p. 93-116.
42. McMahon, S., Koltzenburg, M, Wall, PD, *Wall and Melzack's Textbook of Pain*. 5 ed, ed. M. Stephen B. McMahon, M.D. Koltzenburg, Patrick D. Wall. 2005, New York: Elsevier.
43. Warman, E.N., W.M. Grill, and D. Durand, *Modeling the effects of electric fields on nerve fibers: determination of excitation thresholds*. IEEE Trans Biomed Eng, 1992. **39**(12): p. 1244-54.
44. Rubinstein, J.T., *Axon termination conditions for electrical stimulation*. IEEE Trans Biomed Eng, 1993. **40**(7): p. 654-63.
45. Joshi, R.P., Feng C., Rogers, W.R., *Modeling electrode-based stimulation of muscle and nerve by ultrashort electric pulses*. IEEE Transactions on Plasma Science, 2004. **32**(4): p. 1687- 1695.
46. Novotny, G.E. and E. Gommert-Novotny, *Intraepidermal nerves in human digital skin*. Cell Tissue Res, 1988. **254**(1): p. 111-7.
47. Wallengren, J., *Vasoactive peptides in the skin*. J Investig Dermatol Symp Proc, 1997. **2**(1): p. 49-55.
48. Kennedy, W.R., G. Wendelschafer-Crabb, and T. Johnson, *Quantitation of epidermal nerves in diabetic neuropathy*. Neurology, 1996. **47**(4): p. 1042-8.
49. Lauria, G., et al., *Epidermal innervation: changes with aging, topographic location, and in sensory neuropathy*. J Neurol Sci, 1999. **164**(2): p. 172-8.
50. Peng, Y.B., et al., *Electrophysiological assessment of the cutaneous arborization of Adelta-fiber nociceptors*. J Neurophysiol, 1999. **82**(3): p. 1164-77.
51. McNeal, D.R., *Analysis of a model for excitation of myelinated nerve*. IEEE Trans Biomed Eng, 1976. **23**(4): p. 329-37.
52. MacIver, M.B. and D.L. Tanelian, *Free nerve ending terminal morphology is fiber type specific for A delta and C fibers innervating rabbit corneal epithelium*. J Neurophysiol, 1993. **69**(5): p. 1779-83.